Biocompatibility and toxicity of graphene quantum dots for potential application in photodynamic therapy

Tanveer A. Tabish[1], Chris J. Scotton[2],*, Daniel C. Ferguson[2], Liangxu Lin[1], Anienke van der Veen[2], Sophie Lowry[2], Muhammad Ali[3], Farhat Jabeen[3], Muhammad Ali[4], Paul G. Winyard [2],*, and Shaowei Zhang [1],*

[1] College of Engineering, Mathematics and Physical Sciences, University of Exeter, Stocker Road, Exeter, EX4 4QF United Kingdom

[2] Institute of Biomedical and Clinical Science, University of Exeter Medical School, St Luke's Campus, EX1 2LU, United Kingdom

[3] Department of Zoology, Government College University, Faisalabad, 38000, Pakistan

[4] Faculty of Animal Sciences, Bahauddin Zakariya University, Multan, 60800, Pakistan

*Correspondence; c.j.scotton@exeter.ac.uk, p.g.winyard@exeter.ac.uk, s.zhang@exeter.ac.uk

Abstract:

Aim: Achieving reliably high production of reactive oxygen species (ROS) in photodynamic therapy (PDT) remains challenging. Graphene quantum dots (GQD) hold great promise for PDT. However, the photochemical processes leading to GQD-derived ROS generation have not yet been fully elucidated. **Materials & methods:** Physicochemical characteristics of GQDs were comprehensively investigated, including electron paramagnetic resonance analysis of singlet oxygen production. Dark toxicity was assessed *in vitro* and *in vivo*. **Results:** GQDs demonstrated excellent photo-luminescent features, corrosion resistance, high water solubility, high photo/pH-stability, *in vitro* and *in vivo* biocompatibility and very efficient singlet oxygen/ROS generation. **Conclusion**: The enhanced ROS generation, combined with good biocompatibility and minimal toxicity *in vitro* and *in vivo* support the potential of GQDs for future PDT application.

Keywords: graphene quantum dots, singlet oxygen, reactive oxygen species, photostability, biocompatability, toxicity, corrosion resistance, photodynamic therapy

1

1. Introduction:

<mark>Cancer accounts for over 8 million deaths annually. Standard treatment options include surgery, radio/chemotherapy and photodynamic therapy (PDT). The latter can be a particularly effective modality in the treatment of superficial tumors such as basal cell carcinoma, but has limitations due to low yields of reactive oxygen species (ROS) plus unwanted side effects.</mark> Therapeutic and diagnostic techniques based on quantum dots (QDs) are emerging as a promising paradigm for the battle against life threatening conditions including cancer, renovascular and cardiovascular disease, intestinal inflammatory bowel disease and neurodegenerative diseases[1-4] **. The wide-ranging biological applications of QDs are due to their unique particle size, excellent photo-physical properties, luminescent features and biocompatibility[5,6] *. The photoluminescence features of QDs derived from radiative recombination result in a long-lived electron-hole pair to produce a metastable state similar to the long-lived triplet state of photosensitisers (PS) and provide a cytotoxic mechanism for the production of singlet oxygen and other ROS [7,8]. Photo-induced electron transfer reactions of QDs have therefore recently been envisioned as potential PS for PDT. PDT is a highly selective approach to ablate tumors, without damaging surrounding tissues. Effective PDT requires three key components: a PS; light and oxygen. The combination of these three leads to the production of ROS. These highly reactive species result in a shift of redox balance and trigger the activation of transcription factors implicated in the initiation of cell death signalling via apoptosis and/or necrosis. The efficacy of PDT mainly relies on the yield of singlet oxygen and other ROS production by a PS and this yield depends on the nature of PS involved[9,10]. Despite several leaps forward, a critical challenge still remains in relation to the inadequate oxygen supply in tumors and incapability of selectively localizing diagnostic probes and drugs at tumors sites for the purposes of early diagnosis and effective treatment[11,12]. One emerging strategy is to synthesize nanoplatforms which may achieve higher ROS yield. However the current applications of QDs are often limited by poor water dispersibility, poor photostability, low singlet oxygen and other ROS generation yield, low biocompatibility, and a lack of imaging and therapeutic functions without attaching biomolecules or antibodies[13,14].

Graphene quantum dots (GQDs) are among the latest frontiers of research on graphene (two dimensional monolayered carbon materials with aromatic substructure) [15] **. They are typically derived from graphene/graphite or other 3D graphitic materials by various approaches and exist as mono or few-layered structures with a lateral dimension up to 100 nm[16]. Lower production of ROS and the intrinsic toxicity of conventional organic photosensitizers such as liposomes and polymeric nanoparticles limit their clinical applications in PDT [17]. GQDs have many advantages over conventional organic photosensitizers, such as chemical inertness, high water solubility, photo-stability, interplay between optoelectronic features and shape/size, good donors in the fluorescence resonance energy transfer process, high stability in physiological conditions, specific accumulation at the target site and facile surface functionalization. These features therefore make GQDs promising candidates in novel delivery systems for target-specific photosensitization [18 ** - 21] due to their photoluminescence (PL) properties[22,23], quantum confinement and edge effects[24]. Considerable efforts are being made to understand the interplay of features such as size and shape, in concert with the type and quantity of additional functional groups, for the generation of PL, as well as capacity to act as energy donors for conventional photosensitizers [16,22-24]. The energy transfer between GQDs and cell molecules, such as triplet oxygen, could potentially induce the generation of reactive oxygen species, thus provoking cellular apoptosis. The light-mediated cytotoxicity of GQDs, together with their energy-donor capacity, could therefore open a new area for GQD research in the life sciences - as direct theranostics or as cofactors or components of conventional photosensitizing agents used in PDT. Recent studies have investigated alternative syntheses and PDT-applicability of GQDs with encouraging results[25-27]. Although promising, GQDs will not achieve broad clinical applicability until concerns have been alleviated about toxicity from long term exposure and quantum yield of ROS, as well as surface dependent therapeutic responses and biological corrosion resistance.

In the present study, we report a robust, smart and highly versatile multifunctional GQD which can be synthesized by exfoliation and disintegration from graphite flakes. We have previously reported a novel effective method to obtain water–soluble GQDs with higher yield (7.1 %), showing a size around 20 nm, and with the majority exhibiting mono-layering [28]. Crucially, we have now demonstrated limited *in vivo*

toxicity after four weeks of high dose administration in rats, and subsequently confirm the enhancement of singlet oxygen and other ROS generation of GQDs. The intensity of the electron paramagnetic resonance (EPR) signal, resulting from singlet oxygen generation, showed an increase which was dependent on the irradiation time. The ROS production from GQDs could potentially allow precise therapeutic dosing. *In vivo* toxicity experiments in rats demonstrate that our GQDs have minimal dark toxicity, which is a key attribute for a photosensitizer for subsequent use in photodynamic therapy. In this study we also have investigated water solubility, corrosion resistance and pH/photo-stability. This study lends further credence to the theranostic potential of GQDs in disease.

2. Experimental section:

Synthesis and Characterization of GQDs: We prepared GQDs from our previous established route by exfoliating and disintegrating graphite flakes [28] (Also see Supplementary note 2). Atomic force microscopy (AFM) micrographs were taken by using a VEECO Dimension 3100 Atomic Force Microscope in a tapping mode with a scan rate of 0.5 Hz. Raman spectra were recorded on a Renishaw Raman spectrometer with a 532 nm laser beam. Ultraviolet-visible (UV/Vis) spectra were recorded by a PerkinElmer Lambda 900 Spectrometer at room temperature. Electrochemical behaviour was examined using a CHI 660C Electrochemical Workstation with a distinctive three-electrode cell: Pt as the auxiliary electrode, Ag/AgCl as the reference electrode and gold as the working electrode (2 mm diameter), in a 0.1 M KCl electrolytic solution. Stability test was performed from 0.2 V to -1.0 V for 2 hours. Impedance measurements were carried out in the frequency range of 100 kHz to 0.1 Hz at OCP with voltage amplitude of 0.005 V. GQDs in water and heavy water solutions were dropped onto the mica substrate followed by drying at 70 °C for 5 h. A digital camera was used to record the images and their contact angles were calculated by PolyPro software package.

In vitro toxicity: Cell proliferation was evaluated with the NIH3T3 mouse fibroblast cell line (purchased from the American Type Culture Collection) and 16HBE14o- human bronchial epithelial cell line (obtained via Dr Jo Porter, University College

4

London). NIH3T3 cells were seeded in DMEM+10% FBS, 16HBEs were seeded in αMEM+10% FBS (Life Technologies, UK), in 24-well plates at a density of 15×10^3 cells per well, and allowed to adhere overnight. Cells were then treated with GQDs diluted in 50 µL tissue culture water (Life Technologies, UK) at concentrations ranging from 1.2 µg/ml up to 100 µg/mL. After 48 hours incubation, cells were trypsinized and counted using a hemocytometer to assess cell number relative to untreated cells.

In vivo toxicity: Sprague-Dawley adult male rats (average age of 6-7 weeks, 230-250g weight) were housed under a standard condition of a 12 hours bright/dark sequence with free access to food. All the investigational protocols and measures were approved by the ethical committee of Government College University, Faisalabad, Pakistan. All animals were arbitrarily divided into four experimental groups (control, low dose (5 mg/kg), medium dose (10mg/kg) and high dose (15 mg/kg) of GQDs), n=8 per group. GQDs were intravenously administrated to the rats for 30 days with a three days pause between each injection (amounting to 8 doses over 30 days). Blood samples were collected at day 1, 15 and 30, from the marginal ear vein, and used for complete blood count (CBC) and determination of selected serum biochemical parameters. Hematological parameters: Red blood cells (RBC); Hematocrit (HCT); Mean corpuscular volume (MCV); mean corpuscular haemoglobin (MCH); Hemoglobin (HGBL); Mean corpuscular hemoglobin concentration (MCHC); Platelets (PLT); Lymphocytes (LYM); Eosinophils (%); Monocytes (%); White blood cells (WBC); and serum biochemical parameters: Cholesterol; triglycerides; Alanine transaminase (ALT); Aspartate transaminase (AST); and Total protein, all analysed in blood samples by using Hitachi 902 automatic analyser (Japan). The harvested heart, liver, lung and kidney were fixed with 4% paraformaldehyde for 5 hours and then dehydrated and processed for histology. 6 µm sections were cut from paraffin blocks using a Reichert microtome and stained with eosin (cytoplasm staining). The stained slides were examined by light microscopy through a 20x and 40x objective lens. A histological analysis of vital organs was performed to determine whether or not the GQDs or the degradation of GQDs caused tissue damage and/or any pathologic impacts such as inflammation or necrosis.

5

Detection of singlet oxygen and other reactive oxygen species: To detect $^1O_2$ and other reactive oxygen species being produced via photochemistry by GQDs, solutions of GQDs were irradiated (λ_{max} = 365 nm, pe300-LED) in the presence of nitroxide spin traps 4-hydroxy-2,2,6,6-tetramethylpiperidine (TMP, a $^1O_2$ trap, Sigma-Aldrich), or 5-(diethoxyphosphoryl)-5-methyl-1-pyrroline-N-oxide (DEPMPO, a $O_2^{\bullet-}$, $^\bullet OH$ and CH_2OH trap, Enzo Life Sciences). Pre- and post-irradiation spectra were acquired at room temperature using a FR30 EPR spectrometer (Jeol Ltd., Welwyn Garden City, UK). Prior to irradiation, each sample was injected in to a Jeol quartz WG-LC-11 flat cell, placed into the EPR cavity and a spectrum was acquired. Samples were then irradiated for a given time, after which a second spectral acquisition was carried out. Spectral acquisition parameters for trapping of $^1O_2$ by TMP were: microwave frequency 9.45 GHz, microwave power 4 mW, centre field 3372 G, sweep width 50 G, sweep time 60 s, time constant 1 s, modulation frequency 25 kHz, modulation width 1.25 G with an average of 3 sweeps. Spectral acquisition parameters for trapping of $O_2^{\bullet-}$ and $^\bullet OH$ by DEPMPO were: microwave frequency 9.45 GHz, microwave power 16 mW, centre field 3372 G, sweep width 150 G, sweep time 60 s, time constant 1 s, modulation frequency 25 kHz, modulation width 0.63 G with an average of 3 sweeps. As a positive control for the generation and detection of $^1O_2$, solutions of protoporphyrin IX (PpIX), a well-known photosensitising agent, were prepared at a concentration of 10 μM, mixed with 50 mM TMP, and irradiated (λ_{max} = 635 nm, 25 J/cm^2, Aktilite CL-16). Spectra were acquired pre- and post-irradiation and the detection of an increased EPR signal confirmed that our detection system was operating as expected. To measure the time-dependent generation of $^1O_2$, GQDs were prepared in H_2O at a concentration of 1.3 mg/ml with 50 mM TMP. Spectra were acquired following the irradiation of separate samples for 0, 2, 5, 10 and 30 minutes, which equates to light doses of 0, 0.24, 0.6, 1.2 and 3.6 J/cm^2, respectively. The generation of $^1O_2$ in D_2O was also measured by EPR. GQDs were prepared in H_2O or D_2O at a concentration of 0.5 mg/ml with 50 mM TMP. Spectra were acquired pre- and post-irradiation (1.8 J/cm^2). Lastly, spectra of GQDs in H_2O (0.5 mg/ml) were acquired in the presence of L-Histidine (25 mM), a $^1O_2$ quencher (1.8 J/cm^2). The positive control for spin trapping by DEPMPO consisted of a hypoxanthine (HX) and xanthine oxidase (XO) system[29,30]. We used a solution containing 50 μM HX, 200 μM DTPA, 20 mM DEPMPO and 0.04 U/ml XO in PBS. Following addition of XO, the solution was

immediately injected into a quartz flat cell and a spectrum was acquired. GQDs (1.3 mg/ml) were mixed with DEPMPO (20 mM) and a spectrum was acquired pre- and post-irradiation (1.8 J/cm^2). An additional mixture, containing GQDs, DEPMPO and DTPA (200 µM) was also made and treated in the same manner.

Statistical Analysis: Statistical analysis was performed between two treatment groups by unpaired Student's t-test, and between multiple treatment groups by one-way analysis of variance (ANOVA) with Tukey post-hoc testing or two-way ANOVA with Bonferroni post-hoc test, using Graphpad Prism 5 software. Results are presented as mean ± s.d, unless otherwise indicated. The value of $p < 0.05$ was considered significant.

3. Results

3.1 Preparation and Basic Characterization of GQDs

GQDs were prepared by following our previously established technique of exfoliating and disintegrating graphite flakes (GFs) [28]. The fundamental mechanism of the synthesis is illustrated in Supplementary Figure 1. The GQDs used herein have an atomic force microscopy (AFM) size around 20-40 nm (**Figure 1a**). AFM of the dispersed GQDs gave an average thickness of ~ 1 nm (**Figure 1a inset**), similar to the majority of other QDs due to equivalent size-dependent luminescent features of these QDs, in combination with intrinsic properties of mono-layered graphene[28,31,32]. GQD crystallization was confirmed by Raman spectroscopy (**Figure 1b**); two characteristic D (defect) and G modes of graphene were determined at around 1354 and 1592 cm^{-1}, respectively. The G peak of the GQDs was slightly blue-shifted from that of pure graphite and chemically-reduced graphene oxide (~1588 cm^{-1}) [33,34], since GQDs prepared via this route have oxidized edges, making them water soluble [28]. The FTIR spectrum had two peaks: an absorption peak centered at 1637 cm^{-1}, and a broad peak at 3402 cm^{-1} revealing O-H bonding (Supplementary **Figure 2a**). The absorptions at 1255 cm^{-1} and 1078 cm^{-1} also revealed the existence of C-H and C-O, respectively. The functional groups (O-H, C-H, and C=C) located at the surface of the GQDs act as a passivation layer. This self-passivated surface layer facilitates the water solubility of GQDs [35,36]. The maximum luminescence peak was centered at

around 460 nm (from 370 - 700 nm) at an excitation wavelength of 360 nm as previously reported by us [28] with quantum yield of 7.12% (Supplementary Table 1 and Supplementary Note 1). The time resolved PL (TRPL, time-correlated single photon counting technique) spectra of the GQDs recorded at 460 nm with 360 nm excitation laser source is shown in Figure 1c. The lifetime of the luminescence can be fitted well with a tri-exponential function: 0.32 (14.2%, we cannot exclude that this fast decay may arise from the instrument response), 2.09 (39.3%) and 5.53 ns (46.5%) respectively. The largely nanosecond decay of luminescence suggests that the GQDs are promising candidate materials for optoelectronic and biologic applications. This synthesis and basic characterization demonstrates the reproducibility of our previously reported novel fabrication route.
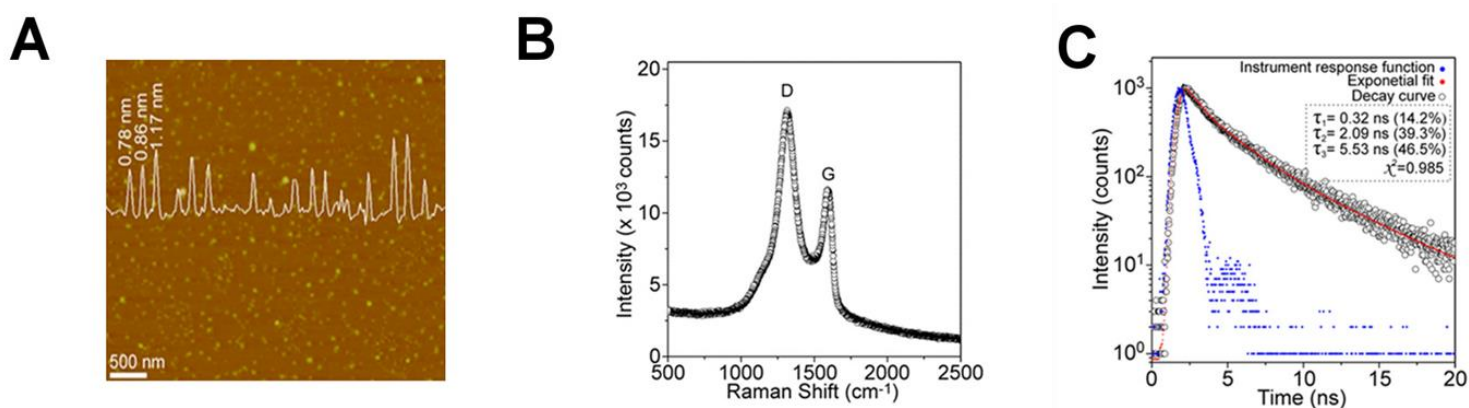

Figure 1. **Basic characterization of GQDs.** (**A**) Representative Atomic Force Microscopy image of GQDs deposited on mica substrate indicating size around 20 - 40 nm, with a particle diameter spectrum showing the complete size distribution of the GQDs (overlaid); (**B**) Raman spectrum demonstrating peaks for D (defect) and G (graphene) at around 1354 and 1592 cm^{-1} respectively; (**C**) Time resolved photoluminescence spectrum of the prepared GQDs, demonstrating the emission lifetime (460 nm) following GQD excitation (360 nm) at room temperature.

3.2 Photo-stability, water dispersibility and pH stability:

The propensity of GQDs for anti-biofouling depends on the physicochemical properties of the QDs surface; key properties include the hydrophilicity of the surface and photo-stability. Incorporation of heavy atoms into the QDs increases the

probability of intersystem crossing and also increases spin orbit coupling of an electron (known as the internal heavy-atom effect). This effect consequently increases the levels of reactive oxygen species generation (see below). Water dispersibility and photo-stability were also measured in heavy water. The water contact angle (CA) was used to evaluate the wettability, hydrophilicity of the GQD surface and water dispersibility. The natural wettability of the surface is reflected by the CA parameter measured immediately through water droplets on the material surface. As shown in **Figure 2 a-b**, the contact angle for water soluble GQDs was 11°, indicating the high hydrophilicity due to the existence of hydrophilic carboxylic groups[37]. The contact angle of 16° for heavy water soluble GQDs was comparable to water soluble GQDs as well as 21.8° on mica substrates. The hydrophilic behaviour of surface amphiphilicity suggested that water and heavy water soluble GQDs both are expected to be an attractive candidate for administration in living systems. The GQDs also showed good water solubility (**Supplementary Figure 3**). To further investigate the effectiveness of GQDs as an optical bio-imaging agent, the stability under various pH conditions was also verified. As shown in **Figure 2 c**, no obvious luminescence quenching of the corresponding PL peak (460 nm) was observed in various buffered solutions, demonstrating that GQDs exhibit no attenuation in PL intensity and that PL is largely independent of pH, which is favourable for bio-imaging applications. Photo-stability was also investigated over a period of >200 hours (**Figure 2 d**), showing that GQDs are highly photo-stable, which is also beneficial for biomedical applications. GQDs exhibited superior photo-stability compared to conventional QDs[38,39]. Overall, the good water dispersibility and solubility, effective pH stability and extraordinary photo-stability render GQDs an attractive alternative probe for efficient imaging in biological and biomedical applications.
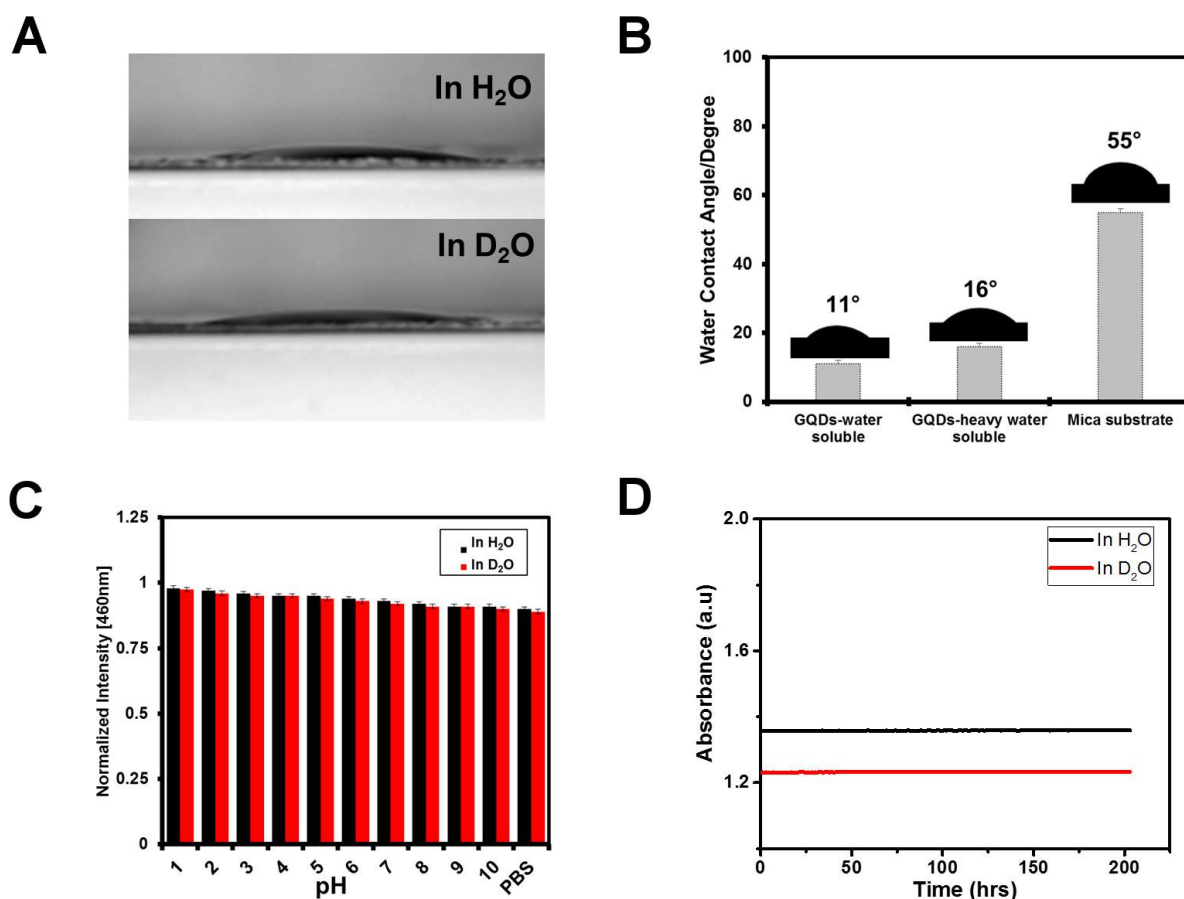
Figure 2. Water dispersibility, pH stability and Photostability of GQDs. (**A, B**) Representative images and quantification of wettability in H_2O and D_2O, as measured by water contact angle, and in comparison with mica substrate; "mica substrate" is the control without GQD. A digital camera was used to record the images and their contact angles were calculated by PolyPro software package. (**C**) pH-stability of GQDs in H_2O and D_2O indicating that no obvious luminescence quenching of the corresponding photoluminescence peak (460 nm) was observed in various buffered solutions (shown as mean ± SD from four different experiments) and (**D**) photostability of GQDs in H_2O and D_2O over a period of 200 hrs.

3. 3 Biological corrosion resistance

Corrosion resistance is known to play an important role in the biocompatibility assessment of bionanomaterials [40,41]. The possible release of metallic ions and particles through electrochemical corrosion phenomena induces inflammatory and toxic effects which in turn reduces the biosafety and biocompatibility of nanomaterials

to solve real-world clinical problems [40,42]. Corrosion resistance depends on morphology and number of layers of quantum dots, exposure environment and electrochemical fluids. It is unclear whether GQDs are resistant to biological corrosion when employed in the context of bio-applications. Biological corrosion occurs in a complex aqueous environment through electrochemical processes,[43] during which GQDs are oxidized to form ions which then migrate away from the GQD surface as free ions[43]. To understand these electrochemical processes, we initially measured their cyclic voltammetry (CV) curves. As shown in **Figure 3a**, CV curves of GQDs had high currents and good rectangular shapes. Pairs of distinctive redox peaks occurred around -8.85 (at 0.098 V, 50 mV.s^{-1}), 11.4 (at 0.151 V, 150 mV.s^{-1}), and -9.57 μA (at -0.171 V, 100 mV.s^{-1}), accompanied with a small redox peak that indicated a multistep glassy carbon ion intercalation/deintercalation[44]. These high redox currents suggested a good corrosion resistance of the GQD passivation layer. They also suggested that the passivation layer on the surface of GQDs could block chemical reactions between the GQDs and body tissues during bio-imaging and therapy treatment, preventing corrosion, and allowing for a potentially longer implantation time. In the CV curve, there was also a small redox peak at ~0.1 V (*vs* Ag/AgCl), most likely arising from the multiple valence states of GQDs. **Figure 3b** shows the stability curve of the GQDs recorded in an electrolytic solution. The stability curve shows a negligible decrease in current density, again indicating excellent stability, even after 2 h of continuous operation. These characteristics of GQDs with active sites can be attributed to the high-temperature-induced strong coordination between the (QDs) surface and electrolyte, and also demonstrates their potential as a sensitive material for electrochemical sensing and bio-imaging. We further used electrochemical impedance spectroscopy (EIS) to monitor the interfacial properties of the self-passivated electrode. The Nyquist plot is shown in **Figure 3c,** revealing a high frequency of electron transfer to the GQD surface, which can be ascribed to the charge-transfer resistance (Rct1= 31.70 Ω) and the double layer capacity (CPE1= 0.05, n=0.542) occurring at the interface between the electrode and the electrolyte[45]. These results confirmed that the network of GQDs provides remarkable electronic conductivity. In this Nyquist plot, the curve at higher frequencies again indicates good corrosion resistance for biological applications[46,47]**.** The potentiodynamic polarization curve of GQDs was also determined (**Figure 3d**); the initial potential was 0.2 V with a corresponding current value of -0.919 μA. The

polarization curve obtained in this study is consistent with literature [40, 48] revealing that polarization plot could be divided in three potential domains: (1) preliminary with the onset of polarization as soon as the GQDs comes in contact with the saline environment; (2) the region having the maximum value of current was labelled as partially active. There was a shift in the corrosion resistance behaviour with a positive potential and current value at -0.999 V and 2.6×10^{-6} A respectively. Furthermore, it was again shifted towards corrosion inhibition at -0.78 V and (3) the formation of the passive layer started with a rise in potential and fall in the current density. This behaviour demonstrated that GQDs act as a corrosion-resistant barrier because a passive layer develops over a short period of time. In addition, these results suggested that the immobilized and passivated GQDs on the electrode could retain their native bioactivity[44].
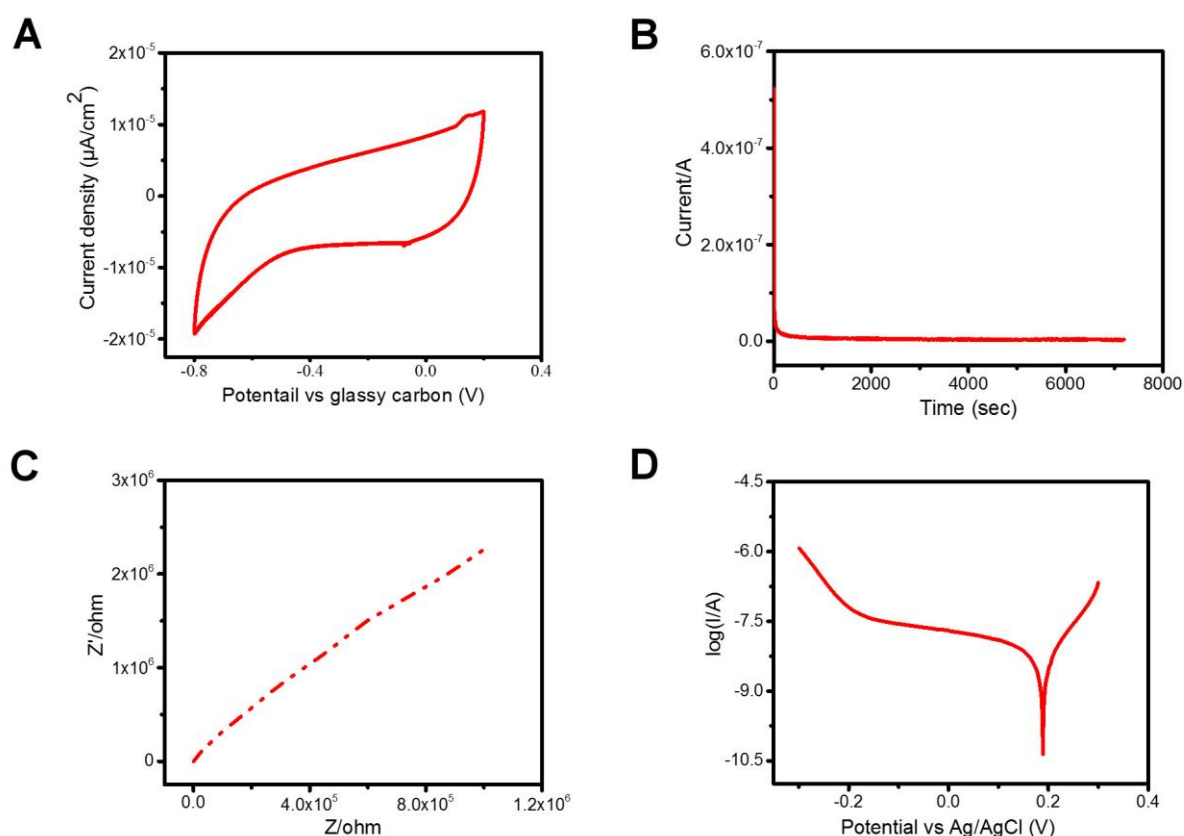
Figure 3. Electrochemical behavior of GQDs in a 0.1 M KCl electrolytic solution. (**A**) CV curves showing the cycle stability at scan rate of 50 mV.s^{-1}; (**B**) stability test performed from 0.2 V to -1.0 V; (**C**) Electrochemical impedance spectroscopy (Nyquist plot) of GQDs. Frequency range: 100 kHz - 0.1 Hz, Voltage amplitude: 0.005 V; (**D**) Potentiodynamic polarization curve.
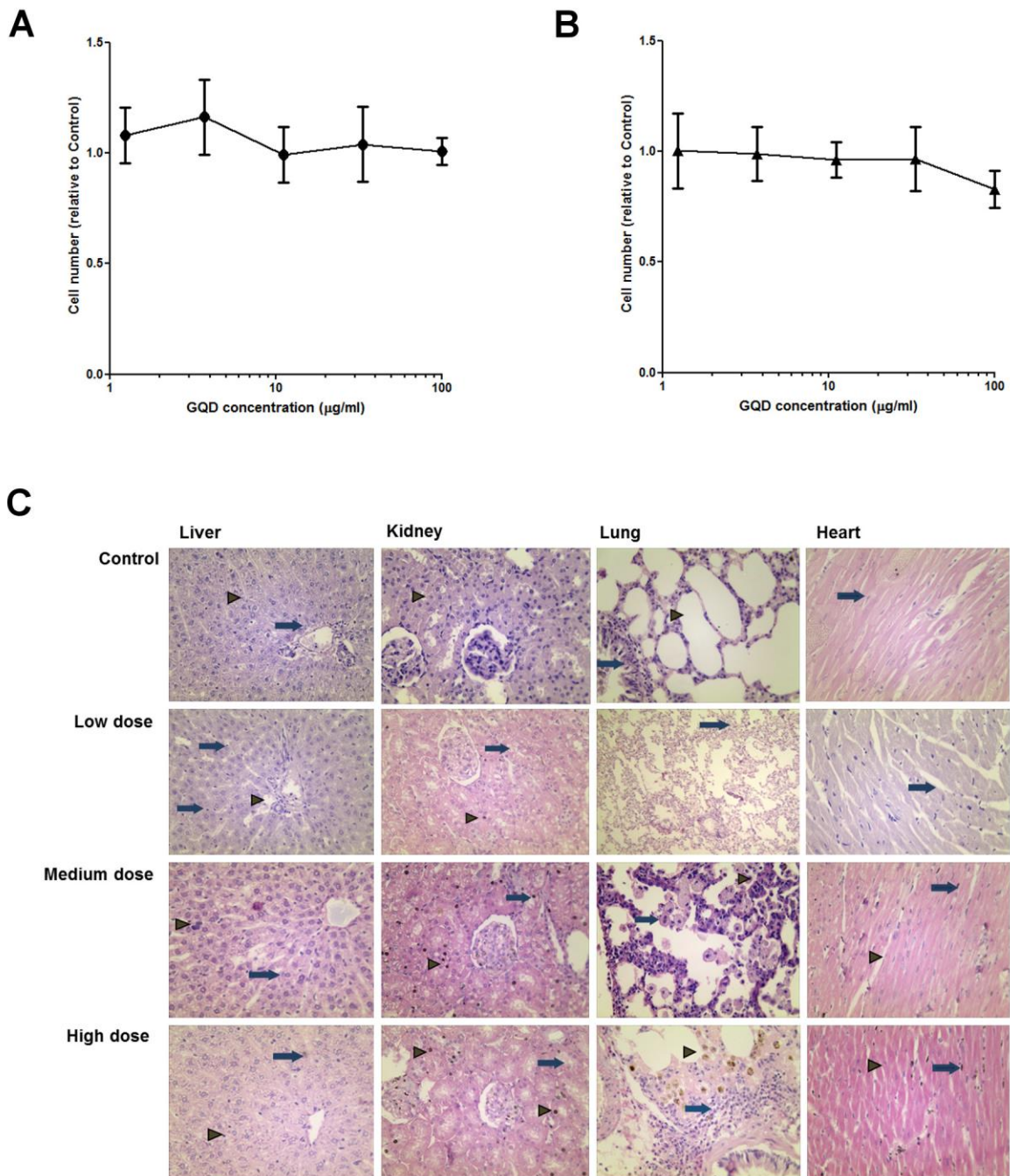
3.4 *In vitro* and *In vivo* cytotoxicity:

The toxicity and biosafety of GQDs has not yet been comprehensively examined[49] and uncertainties remain about how such nanomaterials interact with biological substrates, since this is also dependent on the particular physicochemical characteristics of different formulations. *In vivo* toxicity will further depend on pharmacokinetic and pharmacodynamic parameters as influenced by the route of administration, dose and time period of exposure. *In vitro* cell viability testing using GQDs at concentrations ranging from 1.2 – 100 µg/ml demonstrated no obvious toxicity following a 48 hr incubation with either a human bronchial epithelial cell line, 16HBE14o⁻, or murine NIH3T3 fibroblasts (**Figure 4 a and b**); both cell types continued to proliferate in the presence of GQDs.

To examine the *in vivo* cytotoxicity of GQDs, we performed a complete blood count (CBC), serum biochemistry and histological study of vital organs of control and treated rats in a dose-dependent manner (8 doses spread over a 30 day period of either 5, 10 or 15 mg/kg GQD). No clear toxic effect of GQDs on CBC was observed (**Supplementary Figure 4 a-l**) although there was a slight 6% reduction in platelet numbers in the 10 mg/kg group at 1 week, which normalised by weeks 3 and 4; monocyte and eosinophil fractions similarly underwent a modest dose-dependent reduction, although the proportion of lymphocytes remained stable and total white cell count was unaffected. When serum biochemical parameters were compared between the groups, the results similarly did not indicate any acute toxicity. An increase in total protein was observed at 4 weeks (for all three doses), although the levels remained within the normal range (**Supplementary Information, Figure 5 a-e**).

A comprehensive post mortem histological study was then performed to assess any tissue interactions with GQDs. Sections of heart, kidney, liver and lung were examined for histopathological changes thirty days after GQD administration (at doses of 5, 10 and 15 mg/kg GQD). No gross abnormalities were observed, although some minor changes were particularly noted in the liver and lungs at the 10 and 15 mg/kg doses of GQDs (**Figure 3b** and supplementary table 2 and 3 corresponding to their histological findings). No significant cardiac histology changes were evident. In the liver, some apoptotic bodies, binuclear hepatocytes, and activated Kupffer cells

13

were identified, indicating minor alterations to liver histology, but no infiltration of polymorphic inflammatory cells; hepatocyte swelling due to hepatic sinusoidal obstruction syndrome suggests some pathological effects related to GQDs. A small degree of pigmentation was observed in the kidneys of rats treated with GQDs, possibly indicating lipofuscin deposition, but again no infiltration of inflammatory cells. Within the lungs, occasional giant histiocytes were observed, associated with an inflammatory cell infiltrate, potentially indicative of a mild foreign body reaction to the GQDs. Taken together, these data indicate that GQD treatment did not result in overt acute toxicity, although the minor histopathological changes, particularly in the liver and lungs, warrant long-term observation in future studies.

Figure 4. *In vitro* and *in vivo* toxicity of GQDs. (**A**) Effect of GQDs on human bronchial epithelial cell (16HBE14o-) viability after 48 hours incubation, relative to untreated control cells; (**B**) Effect of GQDs on murine fibroblast (NIH3T3) viability after 48 hours incubation, relative to untreated control cells. Data were analysed by one-way ANOVA with a Tukey multiple comparisons test; no significant differences were observed; (**C**) Histological evaluation of the vital organs of rats at 4 weeks after intravenous injection of GQDs. Tissues of low, medium and high dose of GQD-treated rats were similar to those of the control group. In the control livers, hepatocytes were arranged in cord like pattern (arrowhead). In this section, the

hepatic triad is marked as arrow. Following low dose GQDs, Kupffer cells were evident (arrow). At medium dose GQD, some apoptotic bodies were evident (arrowhead) and occasional binuclear hepatocytes were also seen (arrow). At the high dose of GQDs, no infiltration of polymorphic inflammatory cells was seen; Kupffer cells were still evident (arrowhead) and some apoptotic bodies were clearly seen (arrow). In the kidney, renal corpuscles are shown, with healthy renal epithelium indicated by an arrowhead. While in low, medium and high dose treated tissues, cytoplasmic vacuolation were seen in renal tubular epithelial cell (arrow) but there was no evidence of inflammatory cells in renal parenchyma. In the control lung, normal alveoli (arrowhead) and bronchioles (arrow) are shown in untreated lung tissue. Some interstitial inflammatory infiltration was seen after low dose GQD (arrow), while giant histiocytes were present in medium dose-treated lung parenchyma (arrow). Pigmented alveolar macrophages were present in high dose GQD lung tissue (arrowhead). In control and low dose heart tissue, myofibers were in a normal arrangement with healthy nuclei (arrow). There was some brown pigmentation present in the parenchyma (arrow) following medium dose GQDs. Healthy nuclei were seen in myofibers (arrowhead) and also some brown pigmentation (arrow) following administration of high dose GQD. Representative images shown (n = 8 rats per group), x200 original magnification.
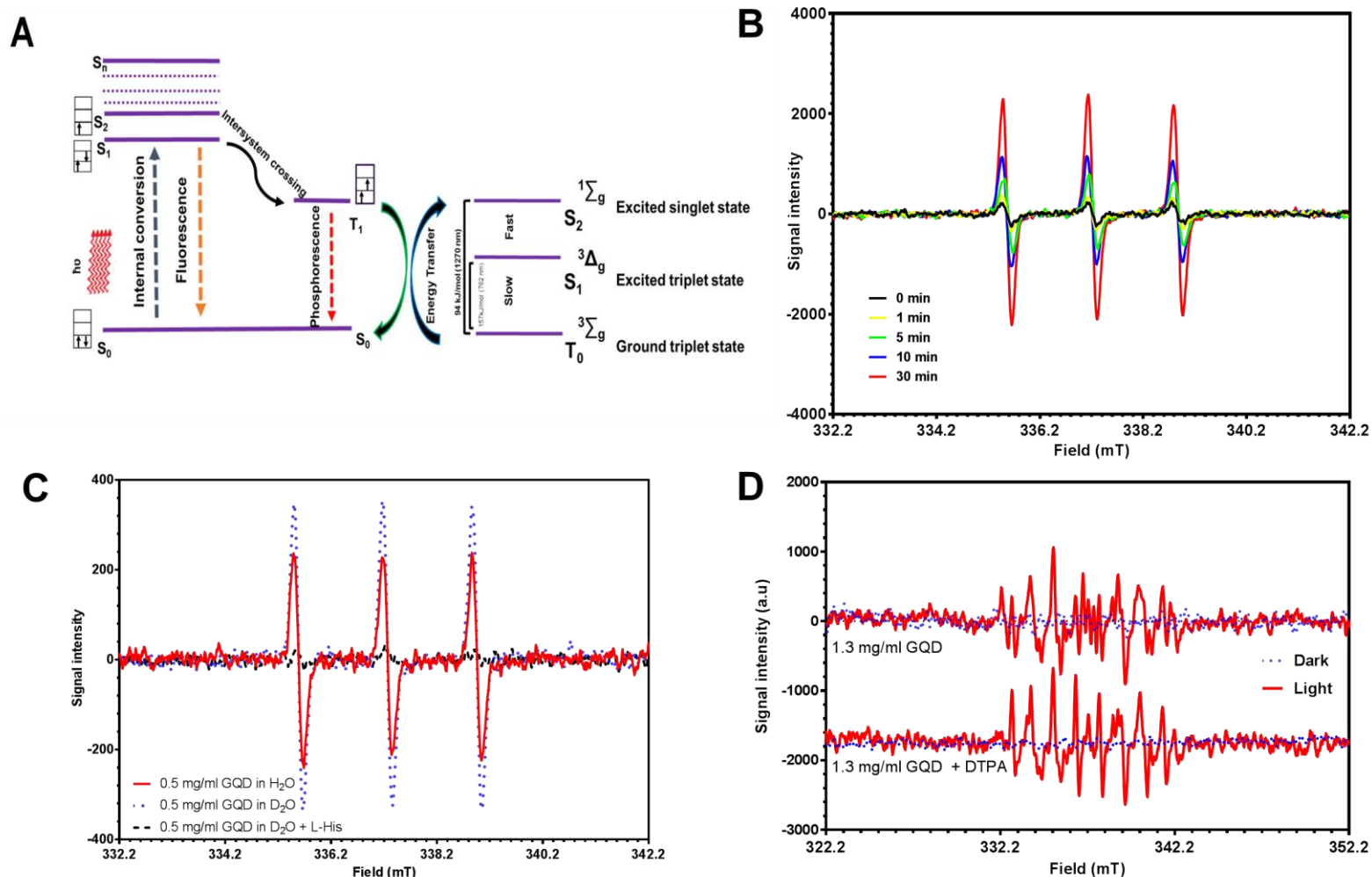
3.5 Singlet oxygen generation and reactive oxygen species:

To further investigate the potential of GQDs for PDT, the singlet oxygen generation capacity of GQDs was verified and their PL in H_2O and D_2O was also measured (Supplementary Figure 6 shows the absorbance and PL of GQDs in H_2O and D_2O.). The lifetime of singlet oxygen in heavy water is 10 times longer than in water[50]; solutions were therefore prepared by adding 0.1 mg of GQD powder into 5 mL of H_2O or 5 mL of D_2O, respectively. It was observed that the blue shift in D_2O was only a little quicker than in H_2O because the singlet oxygen is formed on the GQDs surface by energy transfer from the GQDs. The O_2 molecules involved in oxidation are likely to intercalate onto the surface[50]. Hence, singlet oxygen was responsible for the PL shift of the GQDs. **Figure 5 a** shows a schematic of the mechanism for the singlet oxygen generation from a PDT photosensitizing agent. To further monitor the singlet

oxygen generation, EPR spectra were recorded under different irradiation conditions and it was observed that the intensity of the signal, resulting from singlet oxygen generation, showed an increase which was dependent on the irradiation time (**Figure 5 b**). EPR signals arising from the spin trapping of superoxide were also observed (**Figure 5 c**). These results confirm that energy transfer from GQDs to oxygen is responsible for the excitation of ground state oxygen[51,52]. By utilising the nitroxide spin trap, TMP, in conjunction with EPR spectrometry, we were able to demonstrate that, upon irradiation, GQDs generate $^1O_2$ and that this occurs in a light dose-dependent manner. TMP traps $^1O_2$, producing the stable radical TEMPOL, which has hyperfine splitting of a^N = 16.3. The small TMP signal observed prior to irradiation (0 J/cm^2) was attributable to low-level contamination from the manufacturing process of TMP, as this signal was also observed in solutions of TMP alone (data not shown). As the irradiation time (and thus the light dose) was increased, the concentration of $^1O_2$ generated increased in a linear manner (R^2 = 0.98, data not shown), as indicated by an increasing signal. To further demonstrate that the observed signal(s) were arising from the trapping of $^1O_2$ by TMP, experiments were also carried out in D_2O and in the presence of the $^1O_2$ quencher, L-histidine. When generated in D_2O, $^1O_2$ has a significantly longer lifetime, which was demonstrated here by a 44% increase in the concentration of the TMP reaction product detected post-irradiation. In the presence of L-histidine, no appreciable EPR signal was observed, indicating complete quenching of $^1O_2$ [53,54]. The complete lack of signal, including that arising from the previously described contamination, is likely to be due to the generation of other reactive oxygen species (as described below), which are known to oxidise the product, arising from the reaction of $^1O_2$ with TMP, to the "EPR silent" hydroxylamine form [55]. Thus, in the absence of any $^1O_2$ generation, the signal is completely eliminated. In addition, L-histidine only chemically and physically quenches/captures singlet oxygen and does not do the same with electrons. Thus the formation of the TEMPOL adduct must be caused by singlet oxygen reacting with TMP and not by electron transfer between photoexcited GQDs and TMP. If a proportion of the adduct formation was caused by electron transfer, then we would expect to see a decreased signal, not the complete absence of a signal that we observed with L-histidine. Evidence supports the view that L-histidine does not affect electron transfer [54,55]. We have also established that GQDs generate $O_2^{\cdot-}$ and $^{\cdot}OH$ and during irradiation. Irradiation of GQDs in the presence of DEPMPO

resulted in an EPR signal comprised of the DEPMPO-OOH and DEPMPO-OH spin adducts (a^N = 13.4, a^P = 52.5, a^H = 11.9 and a^N = 14, a^P = 47, a^H = 13; **Figure 5 d**, upper spectrum), indicating the generation of superoxide and hydroxyl radicals, respectively. Addition of the metal chelator DTPA inhibited the generation of hydroxyl radicals [56], leaving the DEPMPO-OOH signal (a^N = 13.4, a^P = 52.5, a^H = 11.9; **Figure 5 d**, lower spectrum).

Figure 5. Singlet oxygen and reactive oxygen species generation by GQDs. (**A**) Schematic diagram of singlet oxygen generation through energy transfer with an excited photosensitizer; this figure has been adopted with permission from reference 9. (**B**) Time-dependent electron paramagnetic resonance signals of GQD solutions mixed with TMP. Signal intensity increased with increasing irradiation time (λ_{max} = 365 nm). (**C**) Electron paramagnetic resonance spectra following irradiation of GQDs (in H_2O and D_2O) in the presence of TMP. Addition of the $^1O_2$ quencher, L-histidine (L-his) completely attenuated the signal. (**D**) Electron paramagnetic resonance spectra of GQDs in DEPMPO. No signals were observed in the dark, but clear signals were observed following irradiation (λ_{max}

= 365 nm) indicating generation of $^\cdot$OH and $O_2^{\cdot-}$. Addition of the transition metal chelator DTPA to remove $^\cdot$OH radicals had little effect on the spectrum, indicating that $O_2^{\cdot-}$ was the dominant species.

4. Discussion:

PDT has been regarded as a minimally invasive treatment modality and widely applied in clinics for various types of cancer treatment [57-58]. Compared to conventional therapies, PDT exhibits certain distinct advantages, since the cytotoxic photosensitizing agent can be selectively activated by manipulating the location of light exposure. However, there are tremendous hurdles to overcome with standard PDT technology because of limited ROS production, lack of deep tissue penetration by the excitation wavelengths utilised, lack of selectivity towards tumor cells and rapid removal from the body. Assembly of luminescent graphene-related materials properties ideal for *in vivo* optical imaging and PDT is therefore highly potential prospect[60,61]. Recent advances in the GQD field have provided unique optical properties, plus remotely controlled release of therapeutic agents *in vitro* and *in vivo*[25,26,62]. The use of any precursor as carbon source and their chemical processing to isolate GQDs, their size tunability and fluorescence quenching can also have a significant effect on ROS generation ability. For example GQDs prepared from graphene oxide are actually graphene oxide QDs and they have different functional groups (such as carbonyl, carboxylic, or hydroxyl groups) as compared to pristine GQDs and which in turn affect the ROS generation and toxicity of GQDs in living systems. Surface functional groups are an especially important parameter in controlling the biological activities of these QDs [9,28,63,64]. In general, several synthesis techniques are available and have been widely used for the preparation of GQDs, such as lithography[65,66], hydrothermal cutting[65,66] and electrochemical preparation[67]. The drawbacks of these methods are the low production yield and the problems associated with the separation and purification of the condensed amorphous carbon phase from low crystalline carbon blacks and fibres[28,49,67]. The resultant product of this partial separation and purification is an oxidized graphite framework and graphene oxide QDs rather than GQDs[65]. Efficient large scale and cost effective production of GQDs remains an important challenge. The features of the different synthetic methods used for the preparation of GQDs have been compared in Supplementary Table 4. Our study demonstrates a novel and facile approach to GQD fabrication through the exfoliation and disintegration of graphite flakes, resulting in GQDs with an excellent repertoire of physicochemical properties, including biocompatibility, water dispersibility, plus high photo and pH stability with

higher quantum yield of 7.12 %, showing a size around 20 nm, and the majority of them are single layered. Further investigation shows that these GQDs exhibit strong luminescence with high quantum yield, which is highly desirable for the real world application of GQDs. Because of the carbene structures in the zigzag planes, the obtained GQDs exhibit exciting luminescence with high quantum yield. On the basis of these fascinating features, GQDs may be optimized for cytocompatibility and surface bioactivity, leading to unique bio-functionality not achieved through existing synthesis approaches. Crucially, they have ideal luminescent features and can generate high yields of singlet oxygen (and other oxygen radicals), above and beyond those currently achievable with state-of-the-art PDT agents. The quantum yield of our GQD preparation compares favourably with that shown in a recent study by Ge et al[25] in which the authors use an alternative strategy for GQD preparation, based on a hydrothermal method using polythiophene derivatives. These two contrasting approaches to GQD fabrication result in nanoparticles with comparable physicochemical properties, indicating that GQDs can be robustly and easily produced with manufacturing processes which could be upscaled for future therapeutic applications while conforming to GMP guidelines. These complementary studies demonstrate that GQDs are therefore highly efficacious for PDT targeting of both cervical carcinoma xenografts in rats and breast cancer xenografts in mice[25], indicating the potentially wide applicability of this technology in a range of tumour types. Building on previous studies, we also investigated the inherent toxicity of GQDs, which is a pivotal consideration for future therapeutic application. Encouragingly, our data indicate that GQDs have minimal toxicity in fibroblasts or epithelial cells cultured *in vitro*. GQDs were then injected at a range of doses into healthy rats, which were monitored over a four week period. The rats had no overt signs of discomfort or ill health. Post mortem analysis revealed only limited histological changes in the liver and lungs, suggestive of a mild inflammatory reaction, but no notable changes were observed in the heart or kidneys. These findings support the biocompatibility of GQDs and alleviate concerns about the toxic side-effects of this treatment approach, although future studies should address long-term toxicology. This investigation also demonstrated that the intensity of the electron paramagnetic resonance signal, resulting from singlet oxygen generation, showed an increase which was dependent on the irradiation time. Singlet oxygen generation was also carried out in D_2O and in the presence of the $^1O_2$ quencher, L-Histidine. When

generated in D_2O, $^1O_2$ has a significantly longer lifetime, which was demonstrated here by a 44% increase in the concentration of TEMPOL detected post-irradiation and the addition of the transition metal chelator DTPA inhibited the production of $^\bullet OH$, leaving a $O_2^{\bullet-}$-specific electron paramagnetic resonance spectrum.

In summary, we have demonstrated a straightforward and facile approach for GQD manufacture, generating GQDs with high singlet oxygen yield, high biocompatibility and corrosion resistance, plus the high photo/pH- stability, indicating their potential as a flexible, multifunctional nanoplatform for cancer therapy. The applications of GQDs are wide-ranging and could be easily extended into other unique functional materials and open new doors for precision nanomedicine in future clinical applications.

5. Conclusion

We herein report the enhanced yield of singlet oxygen and associated ROS from a newly-synthesized GQD with potential as a smart and promising PDT agent. These graphite flake-derived GQDs demonstrated excellent photo-luminescent features, particle diameter, excellent corrosion resistance, high water solubility, high photo/pH-stability, good *in vitro* and *in vivo* biocompatibility and very efficient singlet oxygen/ROS generation. This investigation also demonstrated that the intensity of the electron paramagnetic resonance signal, resulting from singlet oxygen generation, showed an increase which was dependent on the irradiation time.

References:

[1] Choi, H.S., *et al.* Renal clearance of quantum dots. *Nat. biotechnol.* **25,** 1165-1170 (2007)
*** - This is an important study on intravenous administration of quantum dots in rodents and their ultimate renal clearance, filtration and urinary excretion of such nanodots.*

[2] Yaghini, E., Seifalian, A. M., & MacRobert, A. J. Quantum dots and their potential biomedical applications in photosensitization for photodynamic therapy. *Nanomedicine*, 353-363 (2009).
*** - This review presents the potential usefulness of quantum dots as photosensitizer in photodynamic therapy compared with traditional agents such as organic dyes which have low yield of generation of cytotoxic reactive oxygen species.*

[3] Samir, T. M., Mansour, M. M., Kazmierczak, S. C., & Azzazy, H. M. Quantum dots: heralding a brighter future for clinical diagnostics. *Nanomedicine*, *7*(11), 1755-1769 (2012)
*** - This study elucidates the unique features of quantum dots in diagnosis and treatment of different diseases and their clinical challenges to solve real-world problems.*

[4] Bakalova, R., Ohba, H., Zhelev, Z., Ishikawa, M. & Baba, Y. Quantum dots as photosensitizers?. *Nat. biotechnol.* **22,** 1360-1361 (2004)
*** - This study covers the challenges in developing the next generation of photosensitizers for use in photodynamic therapy.*

[5] Cai, W. *et al.* Peptide-labeled near-infrared quantum dots for imaging tumor vasculature in living subjects. *Nano let.* **6**, 669-676 (2006)
** - This paper reports the preparation of arginine-glycine-aspartic acid peptide-labeled quantum dots for use in vivo imaging of tumor vasculature in athymic nude mice following subcutaneous U87MG human glioblastoma tumors and intravenous administration of quantum dots.*

[6] He, X. P., & Tian, H. Photoluminescence Architectures for Disease Diagnosis: From Graphene to Thin-Layer Transition Metal Dichalcogenides and Oxides. *Small*, **12**, 144-160 (2016)
** - This review provides key insights into the recent developments in the synthesis and use of graphene and transition metal dichalcogenides based single-layer materials for single-target and multiplexed detection of a variety of biomarkers and theranostics owing to their low off-target toxicity and therapeutic responses.*

[7] Yaghini, E., Pirker, K. F., Kay, C. W., Seifalian, A. M., & MacRobert, A. J. Quantification of reactive oxygen species generation by photoexcitation of pegylated quantum dots. *Small*, **10**, 5106-5115 (2014)

[8] Yaghini, E., Seifalian, A. M., & MacRobert, A. J. (2009). Quantum dots and their potential biomedical applications in photosensitization for photodynamic therapy.

[9] Tabish, T. A., Zhang, S., & Winyard, P. G. Developing the next generation of graphene-based platforms for cancer therapeutics: The potential role of reactive oxygen species. *Redox Biology*. 34-40 (2018)

[10] Tang, R., Habimana-Griffin, L. M., Lane, D. D., Egbulefu, C., & Achilefu, S. Nanophotosensitive drugs for light-based cancer therapy: what does the future hold? *Nanomedicine*, 1101-1105 (2017)

[11] Ferrari, M. Cancer nanotechnology: opportunities and challenges. *Nat. Rev. Cancer.* **5**, 161-171 (2005)

[12] Ludwig, J.A. & Weinstein, J.N. Biomarkers in cancer staging, prognosis and treatment selection. *Nat. Rev. Cancer.* **5**, 845-856 (2005)

[13] Smith, A.M., Duan, H., Mohs, A.M. & Nie, S. Bioconjugated quantum dots for *in vivo* molecular and cellular imaging. *Adv. drug deliver. Rev.* **60,** 1226-1240 (2008)

[14] Viana, O. S., Ribeiro, M. S., Fontes, A., & Santos, B. S. (2016). Quantum Dots in Photodynamic Therapy. In *Redox-Active Therapeutics* (pp. 525-539). Springer International Publishing.

[15] Kostarelos, K., & Novoselov, K. S. Exploring the interface of graphene and biology. *Science*, *344*(6181), 261-263 (2014).

*** - This article addresses the possible mechanisms of interaction of graphene nanostructures with biological systems. The authors suggest that graphene must be prepared in a biocompatible fashion with variety of their exposure and administration routes in living system to determine their fate.*

[16] Kostarelos, K., & Novoselov, K. S. Graphene devices for life. *Nature nanotech.* *9*(10), 744-745 (2014).

[17] Huynh, E., & Zheng, G. Porphysome nanotechnology: a paradigm shift in lipid-based supramolecular structures. *Nano Today*, *9*(2), 212-222 (2014).

[18] Li, K., Liu, W., Ni, Y., Li, D., Lin, D., Su, Z., & Wei, G. Technical synthesis and biomedical applications of graphene quantum dots. *J. Mater. Chem. B*, 5, 4811-4826 (2017).

*** - This work provides key insights into the synthesis of biocompatible graphene quantum dots for applications in nanomedicine.*

[19] Markovic, Z. M., Ristic, B. Z., Arsikin, K. M., Klisic, D. G., Harhaji-Trajkovic, L. M., Todorovic-Markovic, B. M., & Milivojevic, D. D. Graphene quantum dots as autophagy-inducing photodynamic agents. *Biomaterials*, *33*(29), 7084-7092 (2012).

[20] Tabish, T. A., Pranjol, M. Z. I., Karadag, I., Horsell, D. W., Whatmore, J. L., & Zhang, S. Influence of luminescent graphene quantum dots on trypsin activity. *Intl. J. Nanomedicine*, *13*, 1525-1538 (2018).

[21] Jin, S. H., Kim, D. H., Jun, G. H., Hong, S. H., & Jeon, S. Tuning the photoluminescence of graphene quantum dots through the charge transfer effect of functional groups. *ACS nano*, *7*(2), 1239-1245 (2013).

[22] Zhu, S., *et al*. Surface Chemistry Routes to Modulate the Photoluminescence of Graphene Quantum Dots: From Fluorescence Mechanism to Up-Conversion Bioimaging Applications. *Adv. Funct. Mater.* **22**, 4732-4740 (2012)

[23] Li, L. S. & Yan, X., 2010. Colloidal graphene quantum dots. *J. Phys. Chem. Lett.* **17**, 2572-2576 (2010)

[24] Kim, S. *et al.* Anomalous behaviors of visible luminescence from graphene quantum dots: interplay between size and shape. *ACS nano*, **6**, 8203-8208 (2012)

[25] Ge, J. et al. A graphene quantum dot photodynamic therapy agent with high singlet oxygen generation. *Nature Commun. 5*. (2014).

[26] Du, D., Wang, K., Wen, Y., Li, Y., & Li, Y. Y. Photodynamic Graphene Quantum Dot: Reduction Condition Regulated Photoactivity and Size Dependent Efficacy. *ACS Appl. Mater. Interfaces. 8*, 3287-3294 (2016).

[27] Zhang, D., Wen, L., Huang, R., Wang, H., Hu, X., & Xing, D. Mitochondrial specific photodynamic therapy by rare-earth nanoparticles mediated near-infrared graphene quantum dots. *Biomaterials*, *153*, 14-26 (2018).

[28] Lin, L. & Zhang, S. Creating high yield water soluble luminescent graphene quantum dots via exfoliating and disintegrating carbon nanotubes and graphite flakes. *Chem. Commun.* **48**, 10177-10179 (2012)

[29] Winyard, P., Lunec, J., & Blake, D. Action of free radical generating systems upon the biological and immunological properties of caeruloplasmin. *Int J Biochem*, **16**, 1276 (1984)

[30] Winyard, P. G., Moody, C. J. & Jacob, C. Oxidative activation of antioxidant defence. *Trends Biochem Sci*, **30**, 459 (2005)

[31] Novoselov, K.S. *et al.* Electric field effect in atomically thin carbon films. S*cience*, **306**, 666-669 (2004)

[320] Li, X.; Wang, X.; Zhang, L.; Lee, S & Dai, H. Chemically derived, ultrasmooth graphene nanoribbon semiconductors. *Science*, **319,** 1229-1232 (2008)

[33] Chen, W.; Yan, L. & Bangal, P.R. Chemical reduction of graphene oxide to graphene by sulfur-containing compounds. *J. Phys. Chem. C*, **114,** 19885-19890 (2010)

[34] Lin, L. & Zhang, S. Effective solvothermal deoxidization of graphene oxide using solid sulphur as a reducing agent. *J. Mater. Chem.* **22,** 14385-14393 (2012)

[35] Tang, L. *et al.* Deep Ultraviolet Photoluminescence of Water-Soluble Self-Passivated Graphene Quantum Dots. ACS Nano. **6**, 5102–5110. (2012)

[36] Yao, X., Niu, X., Ma, K., Huang, P., Grothe, J., Kaskel, S. & Zhu, Y. Graphene Quantum Dots-Capped Magnetic Mesoporous Silica Nanoparticles as a Multifunctional Platform for Controlled Drug Delivery, Magnetic Hyperthermia, and Photothermal Therapy. *Small*, *13*. (2017).

[37] Zeng, Z. *et al.* Graphene Oxide Quantum Dots Covalently Functionalized PVDF Membrane with Significantly-Enhanced Bactericidal and Antibiofouling Performances. *Sci. rep.* 6. (2016)

[38] Krishna, K. V., Ménard-Moyon, C., Verma, S., & Bianco, A. Graphene-based nanomaterials for nanobiotechnology and biomedical applications. *Nanomedicine*, *8*(10), 1669-1688 (2013).

[39] Li, L. L. *et al.* Focusing on luminescent graphene quantum dots: current status and future perspectives. Nanoscale **5**, 4015–4039 (2013)

[40] Mazare, Anca, et al. Corrosion, antibacterial activity and haemocompatibility of TiO_2 nanotubes as a function of their annealing temperature. *Corros. Sci.*, 103, 215-222 (2016)

[41] Hamouda, I. M. Current perspectives of nanoparticles in medical and dental biomaterials. *J biomed res, 26*(3), 143-151 (2012)

[42] Kulkarni, M., Mazare, A., Gongadze, E., Perutkova, Š., Kralj-Iglič, V., Milošev, I., & Mozetič, M. Titanium nanostructures for biomedical applications. *Nanotechnology*, *26*(6), 062002 (2015)

[43] Zheng, X. T., Ananthanarayanan, A., Luo, K. Q. & Chen, P. Glowing graphene quantum dots and carbon dots: properties, syntheses, and biological applications. *Small*, **11**, 1620-1636 (2015)

[44] Zhang, W.; Lee, S.; McNear, K.L.; Chung, T.F.; Lee, S.; Lee, K.; Crist, S.A.; Ratliff, T.L.; Zhong, Z.; Chen, Y.P. & Yang, C. Use of graphene as protection film in biological environments. *Sci. rep.* **4**, (2014)

[45] Roushani, M. & Abdi, Z. Novel electrochemical sensor based on graphene quantum dots/riboflavin nanocomposite for the detection of persulfate. *Sensor Actuat. B-Chem.* **201**, 503-510 (2014)

[46] Vasilescu, I. *et al.* Molybdenum disulphide and graphene quantum dots as electrode modifiers for laccase biosensor. *Biosens. Bioelectron.* **75**, 232-237 (2016)

[47] Poznyak, S. K. *et al.* Size-dependent electrochemical behavior of thiol-capped CdTe nanocrystals in aqueous solution. *J. Phys. Chem. B.* **109**, 1094-1100 (2005)

[48] G. Bolat, J. Izquierdo, T. Gloriant, R. Chelariu, D. Mareci, R.M. SoutoInvestigation of processing effects on the corrosion resistance of Ti20Mo alloy in saline solutions. *Corros. Sci.*, 98, 170-179 (2015)

[49] Tabish, T. A., Lin, L., Ali, M., Jabeen, F., Iqbal, R., Horsell, D. W., & Zhang, S. (2018). Investigating the bioavailability of graphene quantum dots in lung tissues via Fourier transform infrared spectroscopy. *Interface focus*, *8*(3), p. 20170054.

[50] Zhang, Y. *et al.* Time-dependent photoluminescence blue shift of the quantum dots in living cells: effect of oxidation by singlet oxygen. *J. Am. Chem. Soc.* **128**, 13396-13401 (2006)

[51] Poznyak, S. K. *et al.* Size-dependent electrochemical behavior of thiol-capped CdTe nanocrystals in aqueous solution. *J. Phys. Chem. B*, 109, 1094-1100 (2005)

[52] Castano, A. P., Mroz, P. and Hamblin, M. R. Photodynamic therapy and anti-tumor immunity. *Nat. Rev. Cancer*, **6**, 535-545 (2006).

[53] Wilkinson, F., Helman, W. P., & Ross, A. B. Rate constants for the decay and reactions of the lowest electronically excited singlet state of molecular oxygen in solution. An expanded and revised compilation. *Journal of Physical and Chemical Reference Data*, *24*(2), 663-677 (1995).

[54] Michaeli A, Feitelson J. Reactivity of singlet oxygen toward amino acids and peptides. *Photochem Photobiol.* 59:284-298 (1994).

[55] Winyard, P., Lunec, J., & Blake, D. (1984). Action of free radical generating systems upon the biological and immunological properties of caeruloplasmin. *International Journal of Biochemistry*, *16*(12), 1273-1278.

[56] Frejaville, C., Karoui, H., Tuccio, B., Moigne, F. L., Culcasi, M., Pietri, S., & Tordo, P. 5-(Diethoxyphosphoryl)-5-methyl-1-pyrroline N-oxide: a new efficient phosphorylated nitrone for the in vitro and in vivo spin trapping of oxygen-centered radicals. *J. Med. Chem.* 1995,38, 258-265 (1995).

[57] Gao, X., Cui, Y., Levenson, R.M., Chung, L.W. & Nie, S. *In vivo* cancer targeting and imaging with semiconductor quantum dots. *Nat. biotechnol.* **22**, .969-976 (2004)

[58] Wang, C., Tao, H., Cheng, L. & Liu, Z. Near-infrared light induced *in vivo* photodynamic therapy of cancer based on upconversion nanoparticles. *Biomaterials*, **32**, 6145-6154 (2011)

[59] Chatterjee, D. K., & Yong, Z. Upconverting nanoparticles as nanotransducers for photodynamic therapy in cancer cells. Nanomedicine, 73-82 (2008)

[60] Du, Y. & Guo, S. Chemically doped fluorescent carbon and graphene quantum dots for bioimaging, sensor, catalytic and photoelectronic applications. *Nanoscale* (2016)

[61] Tan, X. *et al.* Electrochemical synthesis of small-sized red fluorescent graphene quantum dots as a bioimaging platform. *Chem. Commun*, **51**, 2544-2546. (2015)

[62] Qu, D., Zheng, M., Li, J., Xie, Z. & Sun, Z. Tailoring color emissions from N-doped graphene quantum dots for bioimaging applications. *Light: Science & Applications*, **4**, 364 (2015)

[63] Sanchez, V. C., Jachak, A., Hurt, R. H., & Kane, A. B. Biological interactions of graphene-family nanomaterials: an interdisciplinary review. *Chemical research in toxicology*, *25*(1), 15-34 (2011).

[64] Shen, H., Zhang, L., Liu, M., & Zhang, Z. Biomedical applications of graphene. *Theranostics*, *2*(3), 283 (2012).

[65] Liu, R., Wu, D., Feng, X., & Müllen, K. Bottom-up fabrication of photoluminescent graphene quantum dots with uniform morphology. *J. Am. Chem. Soc.* **133**, 15221-15223 (2011)

[66] Stampfer, C., Güttinger, J., Molitor, F., Graf, D., Ihn, T., & Ensslin, K. Tunable Coulomb blockade in nanostructured graphene. *Appl. Phys. Lett.* **92**, 012102 (2008)

[67] Tabish, T. A., Pranjol, M. Z. I., Karadag, I., Horsell, D. W., Whatmore, J. L., & Zhang, S. (2018). Influence of luminescent graphene quantum dots on trypsin activity. *International journal of nanomedicine*, *13*, 1525.

[68] Shen, J., Zhu, Y., Yang, X., & Li, C. Graphene quantum dots: emergent nanolights for bioimaging, sensors, catalysis and photovoltaic devices. *Chem. Commun.* **48**, 3686-3699 (2012).